Field and electric potential of conductors with fractal geometry

Thiago A de Assis[1]**, Fernando de B Mota, José G V Miranda, Roberto F S Andrade and Caio M C de Castilho**

Instituto de Física, Universidade Federal da Bahia, Campus Universitário da Federação, 40210-340, Salvador, BA, Brazil

E-mail: thiagoaa@ufba.br

Abstract

In this study, the behavior of the electric field and its potential are investigated in a region bounded by a rough fractal surface and a distant plane. Both boundaries, maintained at distinct potential values, are assumed to be conductors and, as such, the electric potential is obtained by numerically solving Laplace's equation subject to the appropriate Dirichlet's condition. The rough boundaries, generated by the ballistic deposition and fractal Brownian motion methods, are characterized by the values of the surface roughness W and the local fractal dimension $df = 3 - \alpha$, where α is the usual roughness exponent. The equipotential surfaces, obtained from Laplace's equation, are characterized by these same parameters. Results presented show how df depends on the potential value, on the method used to generate the boundary and on W. The behavior of the electric field with respect to the equipotential surface is also considered. Its average intensity was found to increase as a function of the average distance from the equipotential to the fractal boundary; however, its intensity reaches a maximum before decreasing towards an asymptotic constant value, an effect that increases as the value of W increases.

(Some figures in this article are in colour only in the electronic version)

1. Introduction

Despite the significant progress in theoretical methods for dealing with partial differential equations, classical problems in electrostatics remain unsolved. The solutions to these problems are far from trivial and include, for instance, the analytical solutions of Laplace's (or Poisson's) equation, where the boundaries at which the Neumann, Dirichlet or Cauchy

[1] Author to whom any correspondence should be addressed.

conditions are imposed have irregular shapes. Such solutions are of great relevance to a large number of current problems that require knowledge of the local electric field in the vicinity of conducting or semiconducting tips with small protrusions subjected to large potential differences. Examples of practical situations in which such conditions are found include the mounting of many devices such as microwave power amplifying tubes, field emission displays and several kinds of metal or semiconductor emitters, with nanometer size tips [1–5]. With respect to the latter, experiments show that electron emission by materials is extremely localized, confined to regions with irregularities in a nanometric scale, that display some kind of self-similar property in this particular scale [6]. The emission is controlled by externally monitoring extensive parameters of the systems such as voltage and current intensity. From a theoretical point of view, however, it is important to access the local properties resulting from the solution of Laplace's equation. These intensive properties (electric field intensity and current density) are important to enable an analytical calculation of the emission properties of the device to be performed, using, for example, the Fowler–Nordheim equation [7].

Due to the intrinsic analytical difficulties encountered in evaluating the properties of systems with irregular shapes, it has become current practice to resort to numerical procedures, as well as to concepts that are beyond those of Euclidean geometry, in order to investigate such problems. If the system displays scale invariance, concepts of fractal geometry can be used to measure several of its properties, at least for the length interval within which this invariance prevails. Several fractal-based approaches have been applied to analyze properties of several systems from different branches of science, including those that give rise to irregular surfaces [6, 8, 9]. Herein, concepts of self-affinity lead to the definition of several measures such as the roughness exponent and local fractal dimension, Hölder exponent and singularity (or multifractal) spectrum, among others. These factors play an important role in quantifying the irregularity of surfaces and in evaluating whether this irregularity remains the same over all regions.

In previous studies, we have investigated these concepts in order to analyze the scaling behavior of equipotential lines produced by irregular conducting profiles subjected to a potential difference with respect to a distant straight line [10, 11]. The results presented with respect to the behavior of df have been discussed along two distinct perspectives, either by taking a system of fixed size and allowing the roughness property to change or by considering a collection of systems of increasing size.

In this present paper, we return to the first perspective to study the electrical properties of a three-dimensional region in which the lower and upper boundaries are conductors consisting of, respectively, an irregular surface with fractal properties $z_0 = z_0(x, y)$ for which the average of the normal vector to each surface element points along the z-direction, and a distant plane $z_1 = cte$. Periodic conditions are considered along the x and y plane directions. The fractal surfaces are created either by the ballistic deposition (BD) [8] or by the fractional Brownian motion (FBM) methods [9], while the evaluation of the roughness exponents α for the boundary itself and for the equipotential surfaces proceed according to the root mean square (RMS) methodology [9]. The results discussed herein go beyond those previously discussed in two aspects: first, we discuss not only the properties of the equipotential surfaces, but also the magnitude of the electric field; next, as we consider the systems to be of a fixed size, we explore the behavior of the field and its potential with respect to the value of the surface roughness, i.e., the dispersion of the function $z_0 = z_0(x, y)$.

The rest of the the paper is organized in the following manner. In section 2 the methods used for generating fractal surfaces and for unveiling their scaling behavior are discussed. For the sake of clarity, section 3 is divided into two subsections, in which we discuss, respectively, the behavior of equipotential surfaces, and the dependence of the electric field with respect

to the distance to the boundary and the boundary roughness. The final section of the paper summarizes these new results.

2. Methodology

The electrostatic problem to be solved is that of finding the electric potential in a charge-free region, bounded by two conductors that are kept at constant but different potential values. This corresponds to solving Laplace's equation under Dirichlet boundary conditions. As discussed in the introduction, the irregular shape of one of the boundaries precludes the use of analytical methods; therefore, we were obliged to resort to a three-dimensional extension of Liebmann's method [12] to obtain a numerical solution to the problem. This amounts to mapping the domain onto a three-dimensional lattice of points $\vec{r} = i\hat{\mathbf{i}} + j\hat{\mathbf{j}} + k\hat{\mathbf{k}}$, where i, j and k are integer numbers in the interval $[0, L]$, and $\hat{\mathbf{i}}$, $\hat{\mathbf{j}}$ and $\hat{\mathbf{k}}$ are unit vectors along, respectively, the x, y and z positive directions. Following this mapping, length is then measured in terms of grid units and the differential equation is converted into the following set of difference equations for the potential values $\phi_{i,j,k}$ at each point of the grid [12]:

$$\phi_{i,j,k} = \left[\phi_{i-1,j,k} + \phi_{i+1,j,k}\right] K_{\mathrm{I}} + \left[\phi_{i,j-1,k} + \phi_{i,j+1,k}\right] K_{\mathrm{II}} + \left[\phi_{i,j,k-1} + \phi_{i,j,k+1}\right] K_{\mathrm{III}}. \tag{1}$$

In equation (1), i, j and k label the point $\vec{r}$ of the grid, where the potential is calculated, and the vector $\hat{\mathbf{k}}$ is perpendicular to the distant plane. We consider a simple cubic lattice, therefore $K_{\mathrm{I}} = K_{\mathrm{II}} = K_{\mathrm{III}} = \frac{1}{6}$. The fractal surface and the distant plane are maintained at constant potential values of $\phi_0 = 0$ and $\phi_1 = 100$, respectively.

The potential values at the boundary grid points are maintained constant throughout the entire integration process during which the set of equations represented by (1) is iteratively solved until a predefined convergence in the values of $\phi_{i,j,k}$ associated with the off-boundary points is achieved. This criterion may be, for example, when the maximum difference in the potential $\phi_{i,j,k}$ between two successive iterations is less than $10^{-8}\%$. The initial values of $0 < \phi_{i,j,k} < 100$ are irrelevant to the final solution, but an adequate choice may speed up the convergence. As anticipated in the introduction, periodic boundary conditions were imposed along x and y directions, i.e., $\phi_{i,j,k} = \phi_{i+L,j,k} = \phi_{i,j+L,k} = \phi_{i+L,j+L,k}$.

Once the convergence of ϕ within the iterative procedure is achieved, it is possible to interpolate the solution to obtain the potential value at any off-grid point or, inversely, to obtain approximate values for the coordinates associated with a given value of the potential. The quality of these interpolations depends, of course, on the number of points that are used to construct the grid. Thus, it is possible to evaluate a set of equipotential surfaces for any chosen value of ϕ. Let us consider the simple situation in which the potential variation rate between two successive grid points along the $\hat{\mathbf{k}}$ direction is

$$G_\phi = \frac{\phi_{i,j,k+1} - \phi_{i,j,k}}{\Delta k} = \phi_{i,j,k+1} - \phi_{i,j,k}, \tag{2}$$

as $\Delta k = 1$. The potential at an off-grid point $(i, j, k + \mathrm{d}z)$, where i, j and k assume the same values as in (2), and $0 < \mathrm{d}z < 1$, is given by

$$\phi_{i,j,k+\mathrm{d}z} = \phi_{i,j,k} + G_\phi \, \mathrm{d}z. \tag{3}$$

The components of electric field, E_x, E_y and E_z are evaluated in a similar way. First, let us consider the grid points, where it is possible to obtain first order approximations such as:

$$E_x = \frac{\phi_{i+1,j,k} - \phi_{i,j,k}}{\Delta x} = \phi_{i+1,j,k} - \phi_{i,j,k}, \tag{4}$$

with similar expressions for y and z field components.
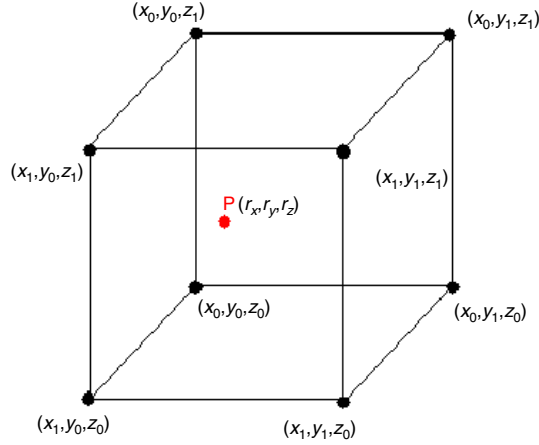
Figure 1. Schematic representation of an off-grid point P, in which the electric field is evaluated.

Let us now consider an off-grid point P, with coordinates (r_x, r_y, r_z), which lies inside a cube, the vertices of which are grid points of coordinates $i + l$, $j + m$ and $k + n$, with $l, m, n = 0, 1$. Using shorthand notation, these coordinates will be expressed as x_n, y_n and z_n, with $n = 0, 1$ (see figure 1). It is possible to evaluate the displacement of P with respect to the coordinated planes passing through the point (x_0, y_0, z_0) by

$$r_{x_0} = x_0 - r_x, \qquad r_{y_0} = y_0 - r_y, \qquad r_{z_0} = z_0 - r_z. \tag{5}$$

As we normalize the distance between any pair of grid points that are first neighbors to 1.0, the displacement of point P to the other seven vertices of the cube can be easily expressed in terms of (5). For instance, the displacement $(r_{x_1}, r_{y_1}, r_{z_1})$, which corresponds to the distance to the coordinated planes passing through (x_1, y_1, z_1) is given by

$$r_{x_1} = 1 - r_{x_0}, \qquad r_{y_1} = 1 - r_{y_0}, \qquad r_{z_1} = 1 - r_{z_0}. \tag{6}$$

Denoting the distance between P and any of the vertices of the cube by $r_{x_n y_n z_n}$, with $n = 0, 1$, so that

$$r_{x_n y_n z_n} = \sqrt{(r_{x_n})^2 + (r_{y_n})^2 + (r_{z_n})^2}, \tag{7}$$

the field components of any off-grid point can be expressed by

$$E_\mu = r_{\text{norm}} \sum_{n=0}^{1} \left[\frac{E_{\mu(i+n, j+n, k+n)}}{r_{x_n y_n z_n}} + \frac{E_{\mu(i+1, j, k+n)}}{r_{x_1 y_0 z_n}} + \frac{E_{\mu(i+n, j+1, k)}}{r_{x_n y_1 z_0}} + \frac{E_{\mu(i, j+n, k+1)}}{r_{x_0 y_n z_1}} \right]. \tag{8}$$

In (8) μ represents x, y or z, and r_{norm} is written as

$$\frac{1}{r_{\text{norm}}} = \sum_{n=0}^{1} \left[\frac{1}{r_{x_n y_n z_n}} + \frac{1}{r_{x_1 y_0 z_n}} + \frac{1}{r_{x_n y_1 z_0}} + \frac{1}{r_{x_0 y_n z_1}} \right]. \tag{9}$$

Let us now consider the fractal analysis, which is used to quantitatively characterize the scaling properties of the irregular sets of the problem: the lower boundary and the equipotential surfaces. As these sets possess self-affine rather than self-similar properties, their scaling behavior may be quantified by the roughness exponent α, which is quite similar to the usual Hurst exponent H [6]. For the current problem, α is a measure of the distinct scales used to leave the system invariant after transformations in the directions perpendicular to the plane and

along the plane. There are several algorithms that may be used to obtain reasonable estimates of the value of α for systems that, like ours, are not exactly invariant according to geometrical construction, but only statistically invariant.

The results reported here were obtained using the root mean square (RMS) method [9], which is based on the scaling behavior of the dispersion of the surface height with respect to the scale h used for the measure. Let $z_{\phi_\ell}(x, y)$ denote the z-coordinate of a generic equipotential surface corresponding to the potential ϕ_ℓ. Note that, within this notation, $z_{\phi=0}(x, y)$ describes the lower boundary of the region. The roughness W of an equipotential, measured in the scale h, is identified by its dispersion $\sigma(h)$ as

$$W(h) = \sigma(h) = \frac{1}{n_h} \sum_{i=1}^{n_h} \sqrt{\frac{1}{m_i} \sum_{x,y \in h} (z_{\phi_\ell}(x, y) - \langle z \rangle)^2}. \tag{10}$$

In (10), $z_{\phi_\ell}(x, y)$ is an equipotential coordinate corresponding to the potential ϕ_ℓ, n_h is the total number of square "windows" of side h, m_i is the number of points within the ith window and $\langle z \rangle$ is the average height of the points corresponding to the equipotential, within the respective "window". For exactly self-affine sets [8] the roughness may be shown to vary asymptotically with the length scale h according to a power law

$$\sigma(h) \approx h^\alpha, \tag{11}$$

where the roughness exponent α is evaluated by fitting the data for $\sigma(h)$. For the problem investigated here, we obtained a series of roughness exponents α_ℓ, which depend on the value of the potential ϕ_ℓ.

Two auxiliary parameters that will be used in the discussion of the results are directly obtained from this method. The first is that the surface roughness W for a patch of area $L \times L$ is defined by $W = \sigma(h_{\max}) = \sigma(L)$. The second is that it should be remembered that it is quite common to associate a local fractal dimension to self-affine objects, which, for irregular surfaces, may be expressed in terms of the roughness exponents α by

$$df = 3 - \alpha. \tag{12}$$

3. Results and discussion

3.1. Scaling properties of equipotential surfaces

In this analysis, irregular boundaries generated by BD and FBM methods are considered. In the first case, there is controversy with respect to the exact value of α, since the best numerical estimates still assign a relatively broad interval $\alpha \in (0.33, 0.4)$ [8, 13]. In the second case, FBM algorithms depend on a free parameter, which allows the possibility of generating *surfaces* with distinct roughness exponents.

In all cases, discrete grids of up to $100 \times 100 \times 100$ points were used. To test the reliability of this code figure 2 shows the $\sigma(h)$ signal plotted as a function of h for three different sets that have been used as boundaries in this electrostatic problem. The values of the exponents α, obtained from a linear regression of each corresponding set of points (see equation (11)), are in agreement with the expected results: one of the surfaces was generated according to the BD algorithm and, accordingly [8], we find $\alpha = 0.331 \pm 0.005$, which leads to $df_B = 2.669 \pm 0.005$. The other two surfaces, grown with the help of an FBM procedure, were selected for having α-values of 0.36 and 0.4, respectively. The slopes of the best linear fits shown in figure 2 indicate $df_{F1} = 2.640 \pm 0.003$ and $df_{F2} = 2.600 \pm 0.002$. Thus, these results validate our code for the RMS algorithm and are used to characterize the set of equipotential surfaces. Although the values of the roughness exponents for the three surfaces lie within a relatively narrow range,
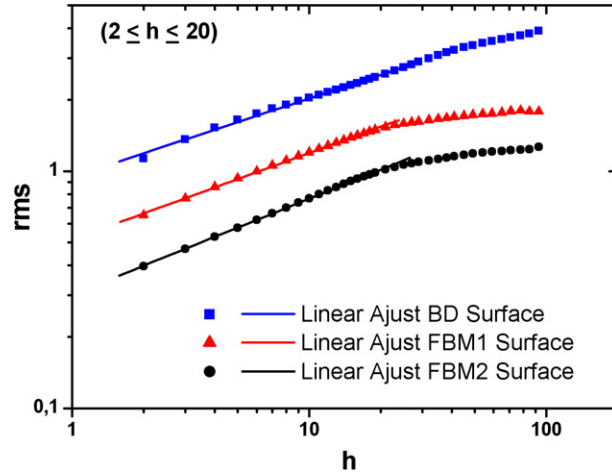
Figure 2. Dependence of $\sigma(h)$ with respect to h for the three different boundaries shown in figure 3. The values of α are similar for the three boundaries, but the roughness value, W, is different. The linear dependence is typical of a self-affine fractal surface. Values of α for the three surfaces were evaluated in the interval $2 \leqslant h \leqslant 20$.
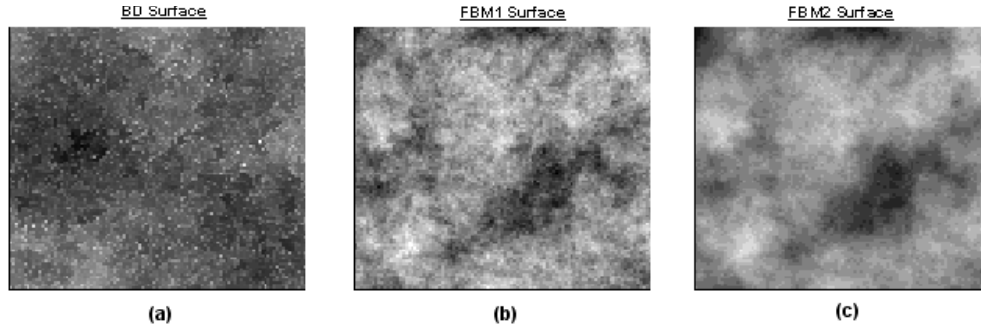

Figure 3. Gray-tone plots of fractal boundary surfaces generated by BD (a) and FBM ((b), (c)) algorithms. Corresponding values of roughness W are 3.89, 1.79 and 1.26. White (black) indicates points with larger (smaller) values of z.

it can be seen that the values of the roughness $W = \sigma(L = 100)$, represented by 3.89, 1.79 and 1.26, respectively, differ considerably from each other, as illustrated in figure 3. This fact, which does not noticeably change the scaling properties of the equipotential surfaces, interferes much more significantly with the properties of the electric field, as will be discussed in the next subsection.

As is already well known, the possibility of lateral attachment during the ballistic deposition process leads to the emergence of voids, located below the points corresponding to the grown surface, as illustrated in figure 4(a). When solving Laplace's equation, the empty sites below the surface are not subject to the boundary conditions and, technically, values of the potential at these points should be evaluated. However, as we have little interest in what happens inside these narrow spaces, we ignored the presence of all empty sites. This is equivalent to considering that all points below the surface have the same potential as the surface, $\phi_{i,j,k_{\mathrm{Sup}}}$, so that

$$\phi_{i,j,k<k_{\mathrm{Sup}}} = \phi_{i,j,k_{\mathrm{Sup}}}. \tag{13}$$
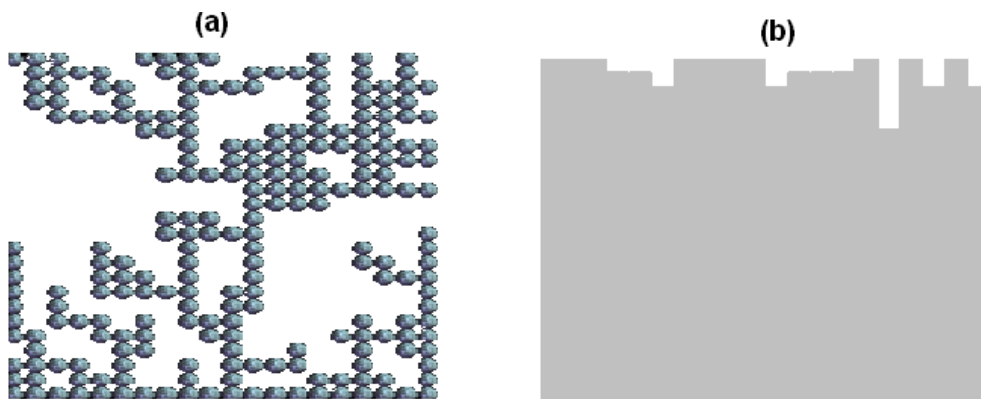
Figure 4. (a) BD showing the lateral attachment that leads to the presence of voids under the surface. (b) Approach used for solving Laplace's equation.
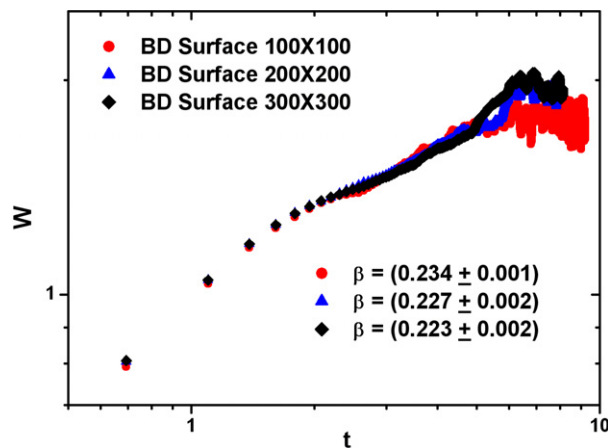

Figure 5. Roughness $W = \sigma(h_{max})$ as a function of deposition time in a logarithmic scale for three different surface sizes in a BD process. After a certain deposition time, W stops increasing. One time unit corresponds to the deposition of the number of particles corresponding to one monolayer.

To complete the characterization of the fractal surfaces acting as boundaries, figure 5 illustrates the growth of W at the early stages of the process of three distinct BD surfaces, from which the growth exponent, β, may be evaluated. Again, the value $\beta \simeq 0.22$ is in agreement with values reported in the literature [8, 14].

The scaling behavior of the equipotential surfaces summarized in figure 6 is now discussed. It illustrates how df_ϕ depends on ϕ when the lower boundary is chosen for each of the surfaces presented in figures 2 and (3). The overall trend shown in figure 6 is the decrease in the value of df_ϕ as ϕ increases; i.e., the equipotential surfaces become less space filling when they approach the smooth upper boundary. Apart from this general feature, it may be seen that, for small values of ϕ ($\leqslant 10$), the variation in df is more pronounced for the BD boundary. For larger values of ϕ, a monotonic decrease in the values of df_ϕ does not change the decreasing order of the values of df that characterizes the lower boundary, i.e., $df_B > df_{F1} > df_{F2}$. These results show that the characteristics of the fractal surface used to form the lower boundary of the region are clearly propagated into the region where the equipotential surfaces are evaluated.
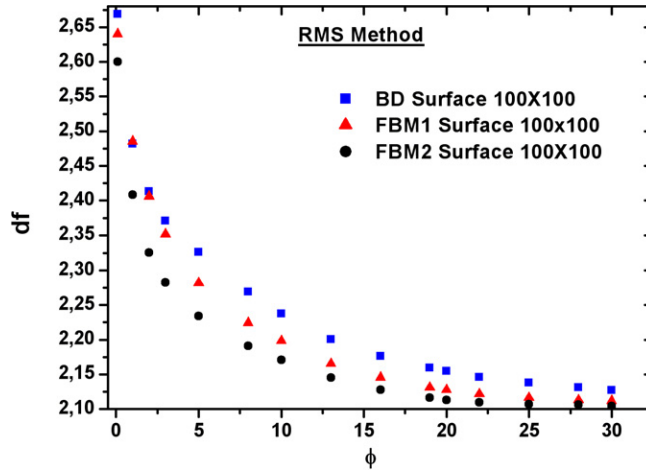
Figure 6. Dependence of df_{ϕ_ℓ}, evaluated for the corresponding equipotential surfaces, as a function of ϕ_ℓ for $0 \leqslant \phi_\ell \leqslant 30$. The lower boundaries are represented by the three fractal surfaces shown in figures 2 and 3. The potential at the lower boundary is set to $\phi = 0.0$, while for the upper boundary, represented by a horizontal distant plane, it is kept at $\phi = 100$ (arbitrary units). df is evaluated according to (10)–(12).

As observed, when analyzing the results for the corresponding one-dimensional problem, we were unable to characterize the dependence of df_ϕ as a function of ϕ by any simple relationship such as an exponential or power law decrease.

The potential value associated with the distant plane is 100 and, of course, this surface has a dimension value of 2.0. Despite its reliability in determining the roughness exponent of an irregular surface [15], the RMS method, as well as other proposed algorithms for measuring scaling behavior, proved to be inadequate for evaluating values of α for flat enough surfaces. Indeed, it is quite easy to notice that, if one tries to apply equations (10) and (11) to a horizontal plane, the value of α is poorly defined. For the set of equipotential surfaces, similar problems occur for $\phi > 30$, particularly when the lower boundary conductor is represented by an FBM surface. This corresponds to the last point of each curve in figure 6, which shows that df_ϕ has reached a value of 2.1. As shown in figure 7, in such a range the values of W drop to less than $1/20$ of their value at $\phi = 0$. In such situations, the correct values of df_ϕ, which decrease continuously to the limit $df_{\phi=100} = 2.0$, cannot be reproduced by the RMS algorithm.

It is also important to discuss the behavior of the average distance $\langle d(\phi_\ell) \rangle$ from a given equipotential surface with $\phi = \phi_\ell$ to the lower fractal boundary. For a system of size $L \times L$, this is defined as

$$\langle d(\phi_\ell) \rangle = \frac{1}{L^2} \sum_{n=1}^{L^2} [z_{\phi_\ell}(x_n, y_n) - z_{\phi=0}(x_n, y_n)]. \qquad (14)$$

Figure 8(a) shows that $\langle d(\phi) \rangle$ depends on the value of ϕ for the same three 100×100 systems as discussed above. The results are similar to those previously calculated for $1D + 1$ profiles [16]. Within a large range of the potential values ($20 \leqslant \phi \leqslant 90$), it is possible to identify a linear dependence between $\langle d(\phi) \rangle$ and ϕ. However, for values of $\phi < 20$, such linear behavior is no longer detected. This is confirmed by examining a neighborhood very close to the lower boundary (see figure 8(b)). For the narrow range of $0.0 < \phi \leqslant 1.0$, a clear non-linear behavior between $\langle d(\phi) \rangle$ and ϕ is found. For graphical convenience, the average distance for
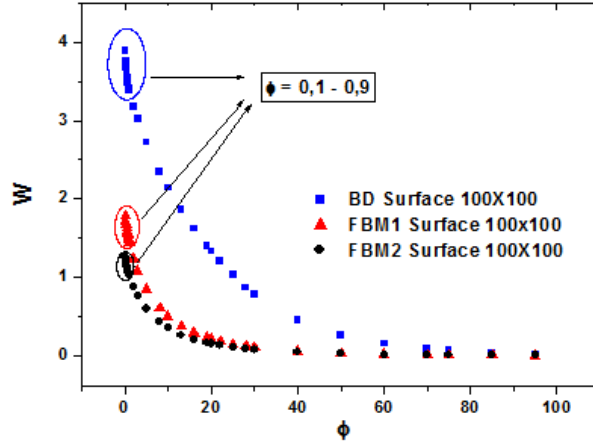
Figure 7. Roughness of the equipotential lines as a function of electric potential for a fractal boundary generated by BD and FBM procedures, with 100×100 dimensions.
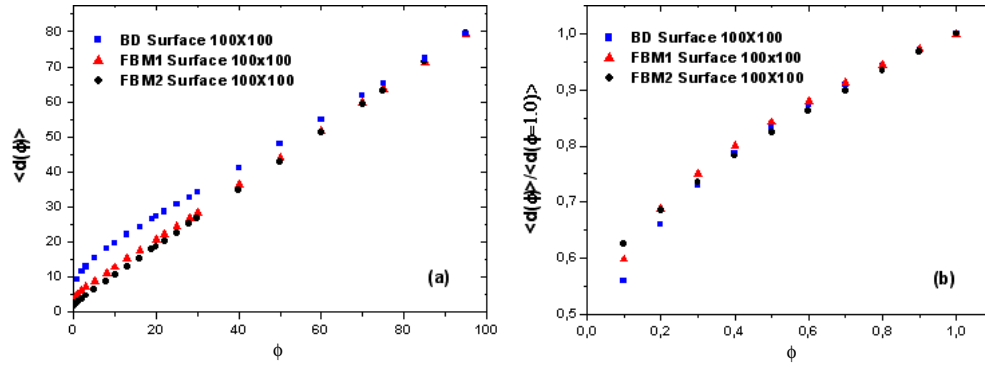
Figure 8. (a) Dependence of $\langle d(\phi) \rangle$ with respect to ϕ. Surfaces shown in figure 3 are used as lower boundaries. (b) Detail of (a) for $0 < \phi \leqslant 1$. For all three boundaries, $\langle d(\phi) \rangle$ is normalized to unity when $\phi = 1.0$.

all three situations was normalized to unity at $\phi = 1.0$. This result is a consequence of an abrupt change in the roughness, as confirmed in figure 7.

3.2. Field properties

Here, changes in the intensity of the electric field are investigated by examining how its mean value along the equipotential surfaces depends on the value of ϕ and on the mean distance from that equipotential surface to the lower boundary $\langle d(\phi) \rangle$. Furthermore, we also discuss how the value of W, for the different fractal surfaces used as lower boundaries, influences the behavior of the electric field.

The average value for the intensity of the electric field associated with an equipotential ϕ_ℓ, i.e. $\langle E(\phi_\ell) \rangle$, is defined by

$$\langle E(\phi_\ell) \rangle = \frac{1}{L^2} \sum_{m=1}^{L^2} [(E_{mx})^2 + (E_{my})^2 + (E_{mz})^2]^{\frac{1}{2}}, \tag{15}$$
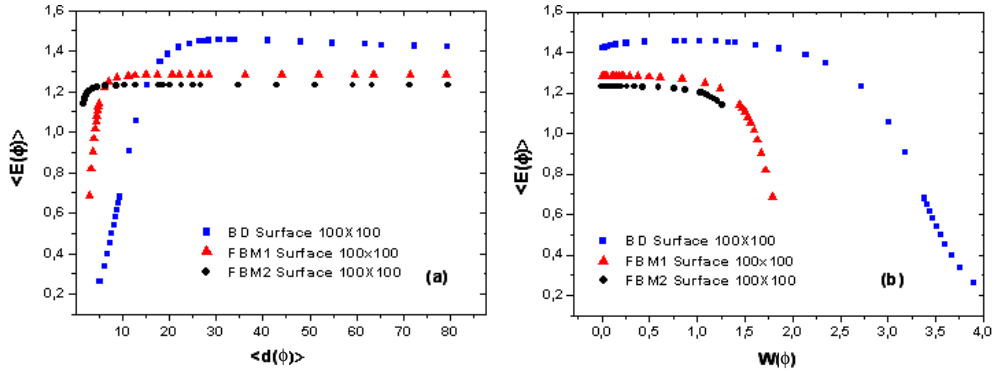
Figure 9. (a) Dependence of $\langle E(\phi)\rangle$ on $\langle d(\phi)\rangle$ for the same boundaries shown in figure 3. As can be seen, the field is very small near the boundary and it converges into a constant value for very large distances. The area under the curve, which corresponds to the potential difference, is the same for all three boundaries used. As (b), the same data for $\langle E(\phi)\rangle$ as in (a), drawn as a function of the roughness $W(\phi)$ of each equipotential surface.

where m runs along the points of the corresponding ϕ_ℓ equipotential surface. For the surfaces used, the average is calculated over 10 000 points.

Figure 9(a) shows how $\langle E(\phi)\rangle$, evaluated at different equipotential surfaces, depends on the value of $\langle d(\phi)\rangle$. The results, which are far from trivial, show that $\langle E(\phi)\rangle$ is very small at points extremely close to the boundary; thereafter, however, undergoing a rapid increase in a relatively narrow interval of $\langle d(\phi)\rangle$. When FBM surfaces, characterized by lower values of W, are taken to form the boundary, the increase in $\langle E(\phi)\rangle$ is still more abrupt if compared with the previous results for the BD boundary. A second interesting aspect shown in figure 9(a) refers to the fact that $\langle E(\phi)\rangle$ goes through a maximum at an intermediate value of $\langle d(\phi)\rangle$.

These two features may be used to compare this behavior to that of a constant field between two parallel plates held at constant potential differences. The electric field results from contributions of the charge distribution over the entire surface. For points that are very close to irregular surfaces, many of these contributions have much larger horizontal components than for a point closer to a flat plane. Moreover, their directions are randomly distributed in the (x, y) plane. These two features lead to small values of the local field intensity and, consequently, to small values of $\langle E(\phi)\rangle$. This explains why the high W boundary sustains very small fields up to larger values of $\langle d(\phi)\rangle$. To emphasize the dependence of $\langle E(\phi)\rangle$ on W, figure 9(b) shows the same data for $\langle E(\phi)\rangle$ as a function of the value of $W(\phi)$ for the corresponding equipotential surface.

The second effect can be more clearly identified for the BD boundary. The average electric field intensity is not constant, but it asymptotically approaches a constant value that depends on the boundary used. This may be easily explained by considering that, despite the fact that the potential bias is the same, the average distance $\langle D\rangle$ between the two corresponding conductors depends on the value of W with respect to the lower boundary. Therefore, $\langle D\rangle$ is smaller for the conductor generated by BD (larger W), which leads to a higher average electric field. The presence of a maximum value of $\langle E(\phi)\rangle$ is correlated to the presence of sharp peaks in the irregular surface. These peaks carry a large charge density that contributes locally to high values of the potential gradient. When the average distance $\langle d(\phi)\rangle$ is larger than the height at which these sharp peak contributions are more relevant, the field starts decreasing to its asymptotic value.

10

If the two boundaries are moved away from each other, corresponding to $W/\langle D \rangle \to 0$, and if there is a corresponding increase in the potential bias, we would finally reach a region where, for each different situation, the field would have the same asymptotic value given by the potential bias divided by $\langle D \rangle$.

4. Summary and conclusions

In this paper we evaluated the electrostatic problem defined in a charge-free region, bounded by two conductors that are kept at a constant potential difference: an irregular surface with fractal properties and a distant plane. The fractal boundaries were generated by the BD and the FBM methods. The purpose of the study was first to characterize the scaling behavior of the equipotential surfaces between the two boundaries.

The dependence of the average electric field is also considered, taken along each of the equipotential surfaces, with respect the mean distance to the irregular boundary and to the surface's own roughness. The RMS method was used for quantifying fractal properties.

Our results show how the fractal dimension df of the equipotential surfaces decreases with the distance to the fractal boundary. This decrease occurs at a slower pace when the region is bounded by the BD surface, even when its fractal dimension is very close to that of a FBM boundary. However, since the roughness, W, of the two surfaces is quite different, this leads to the conclusion that the 'propagation' of the irregularities of the boundary into the bounded region, which is shown by the scaling properties of the equipotential surfaces, depends essentially on W rather than on df.

Investigation of the behavior of the average distance from an equipotential to the fractal boundary $\langle d(\phi) \rangle$, with respect to ϕ, has shown a region of linear variation that does not extend to small values of ϕ. This indicates that, close to the fractal boundary, the gradient of the average distance is no longer constant, as occurs in the case of equipotential surfaces at larger distances from the irregular boundary.

Finally, the average electric field intensity $\langle E(\phi) \rangle$ along an equipotential surface is shown to have a non-trivial dependence on the average distance $\langle d(\phi) \rangle$. For an irregular boundary with a large enough value of W, the value of $\langle E(\phi) \rangle$ reaches a maximum before converging with an asymptotical value at large distances. By comparing the results for boundaries sharing the same value of fractal dimensions, we conclude that this behavior depends greatly on the roughness of the boundary, which, in turn, also depends on the growing process of the fractal boundary.

Acknowledgments

References

[1] Brodie I and Spindt C A 1992 *Adv. Electronics Electron Physics* vol 83, ed P W Hawkes (New York: Academic)
[2] Grigoriev Y A, Petrosyan A I, Penzyakov V V, Pimenov V G, Rogovin V I, Shesterkin V I, Kudryashov V P and Semyonov V C 1997 *J. Vac. Sci. Technol.* B **15** 503
[3] Zhu W, Bower C, Kochanski G P and Jin S 2001 *Solid State Electron.* **45** 921
[4] Isayeva O B, Eliseev M V, Rozhnev A G and Ryskin N M 2001 *Solid State Electron.* **45** 871

 [5] Solnstev V A and Rodionov A N 2001 *Solid State Electron.* **45** 853
 [6] Feder J 1988 *Fractals* (New York: Plenum)
 [7] Fowler R H and Nordheim L W 1928 *Proc. R. Soc.* A **119** 117
 [8] Barabási A L and Stanley H E 1995 *Fractal Concepts in Surface Growth* (Cambridge: Cambridge University Press)
 [9] Russ J C 1994 *Fractal Surfaces* (New York: Plenum)
[10] Cajueiro D O, Sampaio V A A, de Castilho C M C and Andrade R F S 1999 *J. Phys.: Condens. Matter* **11** 4985
[11] Dias Filho H de O, de Castilho C M C, Miranda J G V and Andrade R F S 2004 *Physica* A **342** 388
[12] Gerald C F and Wheatley P O 1985 *Applied Numerical Analysis* 3rd edn (New York: Addison-Wesley)
[13] Haselwandter C A and Vvedensky D D 2006 *Phys. Rev.* E **73** 1539
[14] Souza H C and Mota F B 2003 *Abstracts of VIII Latin American Workshop On Nonlinear Phenomena (Salvador, Brazil)*
[15] de Assis T A 2007 *Master Dissertation* Universidade Federal da Bahia (Salvador, Brazil)
[16] de Assis T A, Mota F B, Miranda J G V, Andrade R F S, Dias Filho H de O and de Castilho C M C 2006 *J. Phys.: Condens. Matter* **18** 3393